# Dynamics of charged-particle between the DC voltage biased plane-parallel conductors

Sung Nae Cho*
*Micro Devices Group, Micro Systems Laboratory, Samsung Advanced Institute of Technology, Samsung Electronics Co., Ltd, Mt. 14-1 Nongseo-dong, Giheung-gu, Yongin-si, Gyeonggi-do 446-712, Republic of Korea.*
(Dated: 8 July 2011)

Analytic description to an oscillating charged-particle between the DC voltage biased plane-parallel conductors is presented. Contrary to the traditional belief in which the oscillation of charged-particle in a uniform DC field is attributed to the reversal in the sign of the particle's charge polarity as it rebounds between the two electrodes, the analytical presentation here reveals no such requirement for the charged-particle oscillation. Since the system involves a spatially oscillating charged-particle, it represents a natural prototype for illuminating electric dipole radiation. By varying the DC bias voltage across the plane-parallel electrodes, the frequency of radiated electromagnetic wave can be adjusted. The device based on charged-particle oscillation is capable of generating coherent electromagnetic waves in the microwave to the X-ray regions of the spectrum, including the technologically important terahertz, infrared, visible, and the ultraviolet wavelengths of the spectrum.



## I. INTRODUCTION

The fact that charged-particle oscillates between the DC voltage biased plane-parallel electrodes is well known[1–3]. Such phenomenon has been extensively studied over years, both theoretically and experimentally, due to its usefulness in variety of applications such as electrostatic thruster and nanoprinting, for instance, which require highly energetic charged-nanoparticles with very high speed[4–8]. Theoretical investigations concerning the phenomenon, so far, have been based on simulations. Although simulation methods often provide a good first-hand understanding of the phenomenon, the interpretation of subtle results can be highly biased whereas no such issue occurs in the analytic investigations as each and every interpretations are based on formidable expressions and not just on the numbers or the plots. For instance, it has been thought that the mechanism responsible for the charged-particle oscillation in a uniform DC field was attributed to the sign reversal occurring in the particle's charge polarity as it rebounds between the two electrodes[9]. The same description based on the analytic theory, however, reveals no such requirement to explain the oscillatory behavior of the charged-particle in a uniform DC field. Moreover, there are situations where oscillating charged-particle rebounds at points sufficiently far from the surfaces of the electrodes. The oscillatory behavior in such situation cannot be explained by the aforementioned description based on the sign reversal of the particle's charge polarity.

In this investigation, an analytic description to the charged-particle oscillation subjected to a uniform DC field is presented. Based on the result, I shall explain that the oscillatory behavior of the charged-particle in a uniform DC field requires a sufficiently large electric field, but does not require the sign reversal in the particle's charge polarity as it rebounds between the DC voltage biased plane-parallel conductors. I shall further conclude that the charged-particle oscillation in a uniform DC field has nothing to do with the sign reversal in the particle's charge polarity. Finally, I shall compare the predicted results from the single charged-particle system considered here with the experiments from the plasma systems.

## II. THEORY

### A. Derivation of electrostatic potentials

The apparatus for the problem is illustrated in Fig. 1(a), where the core-shell structured charged-particle is placed between the plane-parallel conductors subjected to a DC bias voltage across the electrodes. Electrostatic potentials in regions $M_1$, $M_2$, and $M_3$ are described by Laplace equation,

$$\nabla^2 V = 0.$$

In spherical polar coordinate system, Fig. 1(b), Laplace equation reads

$$\frac{1}{r^2}\frac{\partial}{\partial r}\left(r^2\frac{\partial V}{\partial r}\right)+\frac{1}{r^2\sin\theta}\frac{\partial}{\partial\theta}\left(\sin\theta\frac{\partial V}{\partial\theta}\right)+\frac{1}{r^2\sin^2\theta}\frac{\partial^2 V}{\partial\phi^2}=0.$$

For the system with azimuth symmetry, $\partial V/\partial\phi = 0$, Laplace equation reduces to

$$\frac{\partial}{\partial r}\left(r^2\frac{\partial V}{\partial r}\right)+\frac{1}{\sin\theta}\frac{\partial}{\partial\theta}\left(\sin\theta\frac{\partial V}{\partial\theta}\right)=0. \qquad (1)$$

Equation (1) has the general solution given by

$$V(r,\theta)=\sum_{\ell=0}^{\infty}\left(A_\ell r^\ell+\frac{B_\ell}{r^{\ell+1}}\right)P_\ell(\cos\theta),$$

where coefficients $A_\ell$ and $B_\ell$ are constants, and $P_\ell(\cos\theta)$ is the Legendre polynomial of order $\ell$. For regions $M_1$,

$M_2$, and $M_3$ in Fig. 1(a), the electrostatic potentials are given by

$$V_1(r,\theta) = \sum_{\ell=0}^{\infty} A_\ell r^\ell P_\ell(\cos\theta), \tag{2}$$

$$V_2(r,\theta) = \sum_{\ell=0}^{\infty} \left(B_\ell r^\ell + \frac{C_\ell}{r^{\ell+1}}\right) P_\ell(\cos\theta), \tag{3}$$

$$V_3(r,\theta) = \sum_{\ell=0}^{\infty} \left(D_\ell r^\ell + \frac{E_\ell}{r^{\ell+1}}\right) P_\ell(\cos\theta), \tag{4}$$

where coefficients $A_\ell$, $B_\ell$, $C_\ell$, $D_\ell$, and $E_\ell$ are to be joined together by appropriate boundary conditions at the interfaces between regions. Equation (2) does not contain terms like $\sim r^{-\ell-1}$ because these terms blow up at the origin.

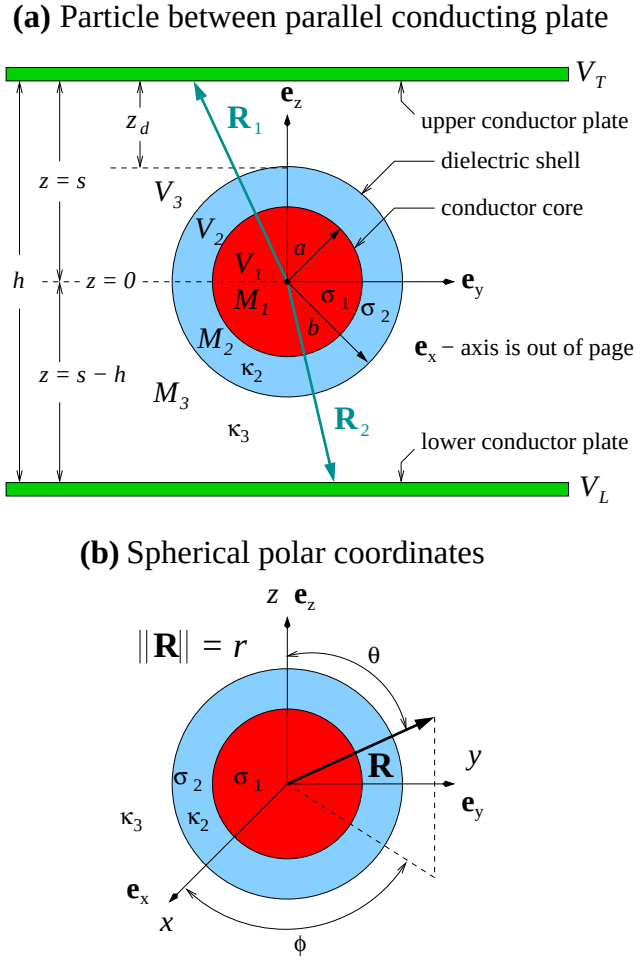


Figure 1: (a) Cross-sectional view of an ionized core-shell structured particle confined by the DC voltage biased plane-parallel conductors. (b) Spherical polar coordinate system showing spherical polar triplet $(r,\theta,\phi)$ of a vector $\mathbf{R}$ in Euclidean three dimensional space, $\mathbb{R}^3$.

Electrostatic potential inside of a conductor is constant; therefore, (2) becomes

$$V_1(r,\theta) = A_0 \equiv V_0, \tag{5}$$

where $V_0$ is a constant. Potential is continuous at $r = a$,

$$V_2(a,\theta) = V_1(a,\theta).$$

From (3) and (5), it can be shown that

$$B_0 + \frac{C_0}{a} + \sum_{\ell=1}^{\infty} \left(B_\ell a^\ell + \frac{C_\ell}{a^{\ell+1}}\right) P_\ell(\cos\theta) = V_0.$$

It follows that coefficient of the like Legendre polynomials are equal, implying $B_0 + C_0 a^{-1} = V_0$ and $B_\ell a^\ell + C_\ell a^{-\ell-1} = 0$. Solving for $C_0$ and $C_\ell$ yields $C_0 = a(V_0 - B_0)$ and $C_{\ell\geq 1} = -B_\ell a^{2\ell+1}$. From these results, (3) becomes

$$V_2(r,\theta) = B_0\left(1 - \frac{a}{r}\right) + \frac{aV_0}{r} + \sum_{\ell=1}^{\infty} B_\ell \left(r^\ell - \frac{a^{2\ell+1}}{r^{\ell+1}}\right) P_\ell(\cos\theta). \tag{6}$$

Equations (4) and (6) must be continuous at $r = b$,

$$V_2(b,\theta) = V_3(b,\theta).$$

With (4) and (6), it can be shown that

$$B_0\left(1 - \frac{a}{b}\right) + \frac{aV_0}{b} + \sum_{\ell=1}^{\infty} B_\ell \left(b^\ell - \frac{a^{2\ell+1}}{b^{\ell+1}}\right) P_\ell(\cos\theta) = D_0 + \frac{E_0}{b} + \sum_{\ell=1}^{\infty} \left(D_\ell b^\ell + \frac{E_\ell}{b^{\ell+1}}\right) P_\ell(\cos\theta).$$

Since the coefficients of the like Legendre polynomials are equal,

$$D_0 + \frac{E_0}{b} = B_0\left(1 - \frac{a}{b}\right) + \frac{aV_0}{b},$$
$$D_\ell b^\ell + \frac{E_\ell}{b^{\ell+1}} = B_\ell\left(b^\ell - \frac{a^{2\ell+1}}{b^{\ell+1}}\right),$$

and the following coefficients are obtained:

$$E_0 = B_0(b-a) + aV_0 - D_0 b,$$
$$E_{\ell\geq 1} = B_\ell\left(b^{2\ell+1} - a^{2\ell+1}\right) - D_\ell b^{2\ell+1}.$$

Using these results, (4) becomes

$$V_3(r,\theta) = D_0\left(1 - \frac{b}{r}\right) + \frac{B_0(b-a) + aV_0}{r} + \sum_{\ell=1}^{\infty}\left[D_\ell\left(r^\ell - \frac{b^{2\ell+1}}{r^{\ell+1}}\right) + \frac{B_\ell\left(b^{2\ell+1} - a^{2\ell+1}\right)}{r^{\ell+1}}\right] P_\ell(\cos\theta). \tag{7}$$

Equation (7) must simultaneously satisfy the boundary conditions at the surfaces of the upper and the lower conductor plates illustrated in Fig. 1(a).

In Cartesian coordinates, the surface of the upper conductor plate is described by the $z = s$ plane and the surface of the lower conductor plate is described by the $z = s - h$ plane. At distances sufficiently far from the particle, the potential inside of the parallel plates can be approximated as

$$V_p = -\int_{s-h}^{z} \mathbf{E}_p \cdot \mathbf{e}_z dz' + V_L,$$

where $V_L$ is the voltage applied to the lower conductor plate, $\mathbf{e}_z$ is the versor along the Cartesian $z$ axis, and $\mathbf{E}_p$ is the electric field inside of the parallel plates in the absence of the charged-particle. The expression for $\mathbf{E}_p$ is given by

$$\mathbf{E}_p = -\mathbf{e}_z \frac{1}{h}\left(V_T - V_L\right), \tag{8}$$

from which the $V_p$ can be obtained:

$$V_p\left(z\right) = E_p\left(z - s + h\right) + V_L, \tag{9}$$

where

$$E_p \equiv \|\mathbf{E}_p\| = \frac{1}{h}\left(|V_T - V_L|\right). \tag{10}$$

In spherical polar coordinate system, the Cartesian coordinate $z$ is represented by $z = r\cos\theta$ and (9) becomes

$$V_p\left(r,\theta\right) = E_p\left(r\cos\theta - s + h\right) + V_L. \tag{11}$$

For $r$ very large, but not infinite in extent, the contributions from terms like $\sim r^{-1}$ and $\sim r^{-\ell-1}$ become negligible in (7) and the $V_3$ takes the form given by

$$V_3\left(r,\theta\right) \approx D_0 + \sum_{\ell=1}^{\infty} D_\ell r^\ell P_\ell\left(\cos\theta\right), \tag{12}$$

where $b \ll r < \infty$. At distances sufficiently far from the particle, $V_3\left(r,\theta\right) \approx V_p\left(r,\theta\right)$. Thus, equating (11) and (12), one obtains

$$\begin{aligned} D_0 + D_1 r\cos\theta + \sum_{\ell=2}^{\infty} D_\ell r^\ell P_\ell\left(\cos\theta\right) \\ \approx E_p r\cos\theta + E_p\left(h - s\right) + V_L. \end{aligned}$$

Matching the coefficients of the like Legendre polynomials yield $D_0 \approx E_p\left(h-s\right) + V_L$, $D_1 \approx E_p$, and $D_{\ell\geq 2} \approx 0$. Using these results, (7) becomes

$$\begin{aligned} V_3\left(r,\theta\right) \approx{}& E_p\left(h-s\right) + V_L + E_p r\cos\theta \\ &+ \left[B_0\left(b-a\right) + aV_0 - bE_p\left(h-s\right) - bV_L\right]\frac{1}{r} \\ &+ \left[B_1\left(b^3 - a^3\right) - b^3 E_p\right]\frac{\cos\theta}{r^2} \\ &+ \sum_{\ell=2}^{\infty} \frac{B_\ell\left(b^{2\ell+1} - a^{2\ell+1}\right)}{r^{\ell+1}} P_\ell\left(\cos\theta\right), \end{aligned} \tag{13}$$

where it is understood that $b \ll r < \infty$. The electrostatic potential, which satisfies the Laplace equation, is a second order differential equation. Therefore, its derivatives must be satisfied at the boundaries. The remaining unknowns, $B_0$, $B_1$, $B_\ell$ for $\ell \geq 2$, and $V_0$ are evaluated from the statement about the continuity of electric displacement at $r = b$ and at $r = a$.

At $r = b$, the normal component of the electric displacement suffers a discontinuity given by

$$\left[\mathbf{e}_r \cdot \mathbf{D}_3\left(r,\theta\right) - \mathbf{e}_r \cdot \mathbf{D}_2\left(r,\theta\right)\right]\big|_{r=b} = \sigma_2, \tag{14}$$

where $\sigma_2$ is the surface free-charge density at $r = b$, the $\mathbf{e}_r$ is a unit vector pointing in the radially outward direction, and $\mathbf{D}_2$ and $\mathbf{D}_3$ represent electric displacements in regions $M_2$ and $M_3$, respectively. In the linear dielectric approximation, the electric displacement can be expressed as

$$\mathbf{D}_i\left(r,\theta\right) = -\epsilon_0 \kappa_i \nabla V_i\left(r,\theta\right), \tag{15}$$

where $\kappa_i$ is the dielectric constant in region $M_i$ and $\epsilon_0$ is the electric permittivity of the free space. Hence, (14) can be expressed as

$$\left[\kappa_2 \mathbf{e}_r \cdot \nabla V_2\left(r,\theta\right) - \kappa_3 \mathbf{e}_r \cdot \nabla V_3\left(r,\theta\right)\right]\big|_{r=b} = \frac{\sigma_2}{\epsilon_0}. \tag{16}$$

In spherical polar coordinate system, the $\nabla$ operator is defined by

$$\nabla = \mathbf{e}_r \frac{\partial}{\partial r} + \mathbf{e}_\theta \frac{1}{r}\frac{\partial}{\partial\theta} + \mathbf{e}_\phi \frac{1}{r\sin\theta}\frac{\partial}{\partial\phi}$$

and (16) becomes

$$\left[\kappa_2 \frac{\partial V_2\left(r,\theta\right)}{\partial r} - \kappa_3 \frac{\partial V_3\left(r,\theta\right)}{\partial r}\right]\Bigg|_{r=b} = \frac{\sigma_2}{\epsilon_0}, \tag{17}$$

which constitutes the Neumann boundary condition at $r = b$. In explicit forms, the derivatives in (17) are evaluated as

$$\begin{aligned} \frac{\partial V_2\left(r,\theta\right)}{\partial r} &= \left(B_0 - V_0\right)\frac{a}{r^2} \\ &+ \sum_{\ell=1}^{\infty} B_\ell\left[\ell r^{\ell-1} + \frac{\left(\ell+1\right)a^{2\ell+1}}{r^{\ell+2}}\right] P_\ell\left(\cos\theta\right) \end{aligned} \tag{18}$$

and

$$\begin{aligned} \frac{\partial V_3\left(r,\theta\right)}{\partial r} &= E_p\cos\theta \\ &- \left[B_0\left(b-a\right) + aV_0 - bE_p\left(h-s\right) - bV_L\right]\frac{1}{r^2} \\ &- 2\left[B_1\left(b^3 - a^3\right) - b^3 E_p\right]\frac{\cos\theta}{r^3} \\ &- \sum_{\ell=2}^{\infty} \frac{\left(\ell+1\right)B_\ell\left(b^{2\ell+1} - a^{2\ell+1}\right)}{r^{\ell+2}} P_\ell\left(\cos\theta\right), \end{aligned} \tag{19}$$

where (6) and (13) have been used. Insertion of (18) and (19) into (17) yields

$$\begin{aligned}\frac{\sigma_2}{\epsilon_0} &= \frac{1}{b^2}\left\{B_0\left[a\left(\kappa_2-\kappa_3\right)+b\kappa_3\right]\right.\\ &\quad \left.-a\left(\kappa_2-\kappa_3\right)V_0-b\kappa_3E_p\left(h-s\right)-b\kappa_3V_L\right\}\\ &\quad +\kappa_3\left\{\frac{2}{b^3}\left[B_1\left(b^3-a^3\right)-b^3E_p\right]-E_p\right\}\cos\theta\\ &\quad +\sum_{\ell=2}^{\infty}B_\ell P_\ell\left(\cos\theta\right)\left\{\frac{\kappa_2\ell}{b^{1-\ell}}\right.\\ &\quad \left.+\frac{\ell+1}{b^{\ell+2}}\left[a^{2\ell+1}\left(\kappa_2-\kappa_3\right)+b^{2\ell+1}\kappa_3\right]\right\}.\end{aligned}$$

Because each Legendre polynomials of order $\ell$ are linearly independent functions, this algebraic relation can be satisfied if and only if the coefficients of each Legendre polynomials vanish independently. Hence,

$$\begin{aligned}B_0\left[a\left(\kappa_2-\kappa_3\right)+b\kappa_3\right]-a\left(\kappa_2-\kappa_3\right)V_0\\ -b\kappa_3\left[E_p\left(h-s\right)+V_L\right]-\frac{b^2\sigma_2}{\epsilon_0}=0,\end{aligned}$$

$$\frac{2}{b^3}\left[B_1\left(b^3-a^3\right)-b^3E_p\right]-E_p=0,$$

$$B_\ell\left\{\frac{\ell+1}{b^{\ell+2}}\left[a^{2\ell+1}\left(\kappa_2-\kappa_3\right)+b^{2\ell+1}\kappa_3\right]+\frac{\kappa_2\ell}{b^{1-\ell}}\right\}=0.$$

One reads off immediately that

$$\begin{aligned}B_0 &= \frac{b\kappa_3\left[E_p\left(h-s\right)+V_L\right]+b^2\epsilon_0^{-1}\sigma_2}{a\left(\kappa_2-\kappa_3\right)+b\kappa_3}\\ &\quad +\frac{a\left(\kappa_2-\kappa_3\right)V_0}{a\left(\kappa_2-\kappa_3\right)+b\kappa_3},\end{aligned}\tag{20}$$

$$B_1=\frac{3b^3E_p}{2\left(b^3-a^3\right)},\tag{21}$$

$$B_\ell=0\ \text{ for }\ \ell\geq 2.\tag{22}$$

With coefficients $B_0$, $B_1$, and $B_{\ell\geq 2}$ defined, (6) and (13) become

$$\begin{aligned}V_2\left(r,\theta\right) &\approx B_0\left(1-\frac{a}{r}\right)+\frac{aV_0}{r}\\ &\quad +B_1\left(1-\frac{a^3}{r^3}\right)r\cos\theta\end{aligned}\tag{23}$$

and

$$\begin{aligned}V_3\left(r,\theta\right) &\approx E_p\left(h-s\right)+V_L+E_pr\cos\theta\\ &\quad +\left[B_0\left(b-a\right)+aV_0-bE_p\left(h-s\right)-bV_L\right]\frac{1}{r}\\ &\quad +\left[B_1\left(b^3-a^3\right)-b^3E_p\right]\frac{\cos\theta}{r^2},\end{aligned}\tag{24}$$

where $V_0$ is the only unknown.

The $V_0$ is evaluated from the statement about the continuity of electric displacement at $r=a$. At $r=a$, the normal component of the electric displacement suffers a discontinuity given by

$$\left[\mathbf{e}_r\cdot\mathbf{D}_2\left(r,\theta\right)-\mathbf{e}_r\cdot\mathbf{D}_1\left(r,\theta\right)\right]\big|_{r=a}=\sigma_1,\tag{25}$$

where $\sigma_1$ is the surface free-charge density at $r=a$ and $\mathbf{D}_1$ is the electric displacement in region $M_1$. Repeating the same procedure outlined from (14) through (17), it can be shown that

$$\left[\kappa_1\frac{\partial V_1\left(r,\theta\right)}{\partial r}-\kappa_2\frac{\partial V_2\left(r,\theta\right)}{\partial r}\right]\Big|_{r=a}=\frac{\sigma_1}{\epsilon_0}.$$

Since region $M_1$ is a conductor, $\partial V_1\left(r,\theta\right)/\partial r=0$ and the Neumann boundary condition at $r=a$ becomes

$$\frac{\partial V_2\left(r,\theta\right)}{\partial r}\Big|_{r=a}=-\frac{\sigma_1}{\epsilon_0\kappa_2}.\tag{26}$$

Using the results in (20), (21), and (22), the derivative in (26) is readily computed from (18),

$$\frac{\partial V_2\left(r,\theta\right)}{\partial r}=\left(B_0-V_0\right)\frac{a}{r^2}+B_1\left(1+\frac{2a^3}{r^3}\right)\cos\theta.$$

With this result, (26) becomes

$$\frac{B_0-V_0}{a}+3B_1\cos\theta=-\frac{\sigma_1}{\epsilon_0\kappa_2}.\tag{27}$$

The $\cos\theta$ in (27) can be eliminated by integrating both sides over the spherical surface at $r=a$,

$$\begin{aligned}\int_{\theta=0}^{\pi}\int_{\phi=0}^{2\pi}\left(\frac{B_0-V_0}{a}+3B_1\cos\theta\right)a^2\sin\theta d\theta d\phi\\ =-\int_{\theta=0}^{\pi}\int_{\phi=0}^{2\pi}\frac{\sigma_1}{\epsilon_0\kappa_2}a^2\sin\theta d\theta d\phi,\end{aligned}$$

yielding

$$B_0-V_0=-\frac{a\sigma_1}{\epsilon_0\kappa_2}.$$

With $B_0$ inserted from (20), $V_0$ can be solved to yield

$$\begin{aligned}V_0 &= V_L+\frac{a\left(b-a\right)\sigma_1}{b\epsilon_0\kappa_2}+\frac{a^2\sigma_1+b^2\sigma_2}{b\epsilon_0\kappa_3}\\ &\quad +E_p\left(h-s\right).\end{aligned}\tag{28}$$

With (28), the coefficient $B_0$ of (20) becomes

$$\begin{aligned}B_0 &= V_L+\frac{a\left(2b-a\right)\sigma_1}{b\epsilon_0\kappa_2}+\frac{a^2\sigma_1+b^2\sigma_2}{b\epsilon_0\kappa_3}\\ &\quad +E_p\left(h-s\right).\end{aligned}\tag{29}$$

With coefficients $B_1$, $V_0$, and $B_0$ defined respectively in (21), (28), and (29), the electrostatic potentials for regions $M_1$, $M_2$, and $M_3$ are obtained from (5), (23), and (24). They are

$$V_1 \approx V_L + \alpha + E_p\left(h-s\right), \tag{30}$$

$$V_2\left(r,\theta\right) \approx V_L + \beta + E_p\left(h-s\right) + \gamma E_p r\cos\theta - \frac{\lambda}{r} - \frac{a^3\gamma E_p\cos\theta}{r^2}, \tag{31}$$

$$V_3\left(r,\theta\right) \approx V_L + E_p\left(h-s\right) + E_p r\cos\theta + \frac{\nu}{r} + \frac{b^3 E_p\cos\theta}{2r^2}, \tag{32}$$

where $\alpha$, $\beta$, $\gamma$, $\lambda$, and $\nu$ are defined as

$$\begin{aligned}
\alpha &= \frac{a\left(b-a\right)\sigma_1}{b\epsilon_0\kappa_2} + \frac{a^2\sigma_1 + b^2\sigma_2}{b\epsilon_0\kappa_3},\\
\beta &= \frac{a\left(2b-a\right)\sigma_1}{b\epsilon_0\kappa_2} + \frac{\left(a^2+b^2\right)\sigma_2}{b\epsilon_0\kappa_3},\\
\gamma &= \frac{3b^3}{2\left(b^3-a^3\right)},\\
\lambda &= \frac{a^2\sigma_1}{\epsilon_0\kappa_2},\\
\nu &= \frac{2a\left(b-a\right)\sigma_1}{\epsilon_0\kappa_2} + \frac{a^2\sigma_1 + b^2\sigma_2}{\epsilon_0\kappa_3}.
\end{aligned} \tag{33}$$

### B. Induced surface charges on conductor plates

In spherical polar coordinate system, $\nabla$ operator is defined by

$$\nabla = \mathbf{e}_r\frac{\partial}{\partial r} + \mathbf{e}_\theta\frac{1}{r}\frac{\partial}{\partial\theta} + \mathbf{e}_\phi\frac{1}{r\sin\theta}\frac{\partial}{\partial\phi},$$

where

$$\begin{aligned}
\mathbf{e}_r &= \mathbf{e}_x\sin\theta\cos\phi + \mathbf{e}_y\sin\theta\sin\phi + \mathbf{e}_z\cos\theta,\\
\mathbf{e}_\theta &= \mathbf{e}_x\cos\theta\cos\phi + \mathbf{e}_y\cos\theta\sin\phi - \mathbf{e}_z\sin\theta,\\
\mathbf{e}_\phi &= -\mathbf{e}_x\sin\phi + \mathbf{e}_y\cos\phi.
\end{aligned}$$

Hence, the $\mathbf{e}_z$ component of $\nabla$ operator is given by

$$\mathbf{e}_z\mathbf{e}_z\cdot\nabla = \mathbf{e}_z\cos\theta\frac{\partial}{\partial r} - \mathbf{e}_z\frac{\sin\theta}{r}\frac{\partial}{\partial\theta}.$$

Using the form defined in (15), the electric displacement in region $M_3$ is given by

$$\mathbf{D}_3\left(r,\theta\right) = -\epsilon_0\kappa_3\nabla V_3\left(r,\theta\right).$$

The $\mathbf{e}_z$ component of $\mathbf{D}_3\left(r,\theta\right)$ is obtained by replacing the $\nabla$ with the $\mathbf{e}_z\mathbf{e}_z\cdot\nabla$ operator and this gives

$$\mathbf{D}_{3;z}\left(r,\theta\right) = \epsilon_0\kappa_3\mathbf{e}_z\left[\frac{\sin\theta}{r}\frac{\partial V_3\left(r,\theta\right)}{\partial\theta} - \cos\theta\frac{\partial V_3\left(r,\theta\right)}{\partial r}\right],$$

where the notation $\mathbf{D}_{3;z}\left(r,\theta\right)$ denotes the $\mathbf{e}_z$ component of $\mathbf{D}_3\left(r,\theta\right)$. With $V_3\left(r,\theta\right)$ of (32), the $\mathbf{e}_z$ component of electric displacement in region $M_3$ is given by

$$\mathbf{D}_{3;z}\left(r,\theta\right) = \left[\frac{\nu}{r^2}\cos\theta + \frac{b^3E_p}{2r^3}\left(3\cos^2\theta-1\right) - E_p\right] \times \epsilon_0\kappa_3\mathbf{e}_z. \tag{34}$$

The surface of the upper conductor plate is described by the Cartesian $z = s$ plane. In the spherical polar coordinate system, the surface of the upper conductor plate is described by

$$\cos\theta = \frac{s}{\sqrt{x^2+y^2+s^2}}.$$

Insertion of the expression for $\cos\theta$ into (34) yields

$$\mathbf{D}_{3;z}\left(x,y,s\right) = \mathbf{e}_z\epsilon_0\kappa_3\left[\frac{3b^3E_ps^2}{2\left(x^2+y^2+s^2\right)^{5/2}} + \frac{2\nu s - b^3E_p}{2\left(x^2+y^2+s^2\right)^{3/2}} - E_p\right]. \tag{35}$$

At the surface of the upper conductor plate, the electric displacement suffers a discontinuity given by

$$\mathbf{e}_z\cdot\mathbf{D}_{ucp;z}\left(x,y,s\right) - \mathbf{e}_z\cdot\mathbf{D}_{3;z}\left(x,y,s\right) = \sigma_{iup}, \tag{36}$$

where $\sigma_{iup}$ is the induced surface charge density on the surface of the upper conductor plate and $\mathbf{D}_{ucp;z}$ is the $\mathbf{e}_z$ component of the electric displacement inside of the upper conductor plate. Since the electric displacement inside of the upper conductor plate is zero, (36) reduces to $\mathbf{e}_z\cdot\mathbf{D}_{3;z}\left(x,y,s\right) = -\sigma_{iup}$ and the surface charge density is given by

$$\sigma_{iup} = -\epsilon_0\kappa_3\left[\frac{3b^3E_ps^2}{2\left(x^2+y^2+s^2\right)^{5/2}} + \frac{2\nu s - b^3E_p}{2\left(x^2+y^2+s^2\right)^{3/2}} - E_p\right], \tag{37}$$

where (35) has been inserted for $\mathbf{D}_{3;z}\left(x,y,s\right)$.

The surface of the lower conductor plate is described by the Cartesian $z = s-h$ plane. In the spherical polar coordinate system, the surface of the lower conductor plate is given by

$$\cos\theta = \frac{s-h}{\sqrt{x^2+y^2+\left(s-h\right)^2}}$$

and (34) becomes

$$\mathbf{D}_{3;z}\left(x,y,s-h\right) = \mathbf{e}_z\epsilon_0\kappa_3\left\{\frac{3b^3E_p\left(s-h\right)^2}{2\left[x^2+y^2+\left(s-h\right)^2\right]^{5/2}} + \frac{2\nu\left(s-h\right) - b^3E_p}{2\left[x^2+y^2+\left(s-h\right)^2\right]^{3/2}} - E_p\right\}. \tag{38}$$

At the surface of the lower conductor plate, the electric displacement suffers a discontinuity given by

$$\mathbf{e}_z\cdot\mathbf{D}_{3;z}\left(x,y,s-h\right)-\mathbf{e}_z\cdot\mathbf{D}_{lcp;z}\left(x,y,s-h\right)=\sigma_{ilp}, \quad (39)$$

where $\sigma_{ilp}$ is the induced surface charge density on the surface of the lower conductor plate and $\mathbf{D}_{lcp;z}$ is the $\mathbf{e}_z$ component of the electric displacement inside of the lower conductor plate. Since the electric displacement inside of the lower conductor plate is zero, (39) reduces to $\mathbf{e}_z\cdot\mathbf{D}_{3;z}\left(x,y,s-h\right)=\sigma_{ilp}$ and, with (38) inserted for $\mathbf{D}_{3;z}\left(x,y,s-h\right)$, the induced surface charge density is given by

$$\sigma_{ilp}=\epsilon_0\kappa_3\left\{\frac{3b^3E_p\left(h-s\right)^2}{2\left[x^2+y^2+\left(h-s\right)^2\right]^{5/2}}-\frac{2\nu\left(h-s\right)+b^3E_p}{2\left[x^2+y^2+\left(h-s\right)^2\right]^{3/2}}-E_p\right\}, \quad (40)$$

where $(s-h)$ has been re-expressed as $-(h-s)$ purely for convenience.

In the limit the parallel plates become infinite in extent, the total of induced charges on the surfaces of each conductor plates must add up to the total charge carried by the particle. To check on this, (37) and (40) are integrated over the surfaces of infinite parallel conductor plates with gap $h$. For convenience, I shall perform the integral in the polar coordinate system. In terms of the polar coordinates, (37) and (40) become

$$\sigma_{iup}\left(\rho,s\right)=-\epsilon_0\kappa_3\left[\frac{3b^3E_ps^2}{2\left(\rho^2+s^2\right)^{5/2}}+\frac{2\nu s-b^3E_p}{2\left(\rho^2+s^2\right)^{3/2}}-E_p\right], \quad (41)$$

$$\sigma_{ilp}\left(\rho,s\right)=\epsilon_0\kappa_3\left\{\frac{3b^3E_p\left(h-s\right)^2}{2\left[\rho^2+\left(h-s\right)^2\right]^{5/2}}-\frac{2\nu\left(h-s\right)+b^3E_p}{2\left[\rho^2+\left(h-s\right)^2\right]^{3/2}}-E_p\right\}, \quad (42)$$

where $\rho\equiv\sqrt{x^2+y^2}$. Since the surface in polar coordinate system is symmetric about its axis, the total induced charges on both conductors can be performed as follow:

$$\begin{aligned}Q_{iT}&=Q_{iup}+Q_{ilp}\\&=\int_{\phi=0}^{2\pi}\int_{\rho=0}^{\infty}\left[\sigma_{iup}\left(\rho,s\right)+\sigma_{ilp}\left(\rho,s\right)\right]\rho d\rho d\phi\\&=2\pi\int_{\rho=0}^{\infty}\left[\sigma_{iup}\left(\rho,s\right)+\sigma_{ilp}\left(\rho,s\right)\right]\rho d\rho,\end{aligned}$$

where $Q_{iup}$ and $Q_{ilp}$ are respectively the total induced charge on the surface of the upper and the lower conductor plates. With (41) and (42), the $Q_{iT}$ becomes

$$\frac{Q_{iT}}{\pi\epsilon_0\kappa_3}=-\int_0^{\infty}\left\{\frac{3b^3E_ps^2}{\left(\rho^2+s^2\right)^{5/2}}-\frac{3b^3E_p\left(h-s\right)^2}{\left[\rho^2+\left(h-s\right)^2\right]^{5/2}}+\frac{2\nu s-b^3E_p}{\left(\rho^2+s^2\right)^{3/2}}+\frac{2\nu\left(h-s\right)+b^3E_p}{\left[\rho^2+\left(h-s\right)^2\right]^{3/2}}\right\}\rho d\rho. \quad (43)$$

Equation (43) involves the following integral types:

$$\int_0^{\infty}\frac{\rho d\rho}{\left(\rho^2+c^2\right)^{3/2}}=-\left.\frac{1}{\sqrt{\rho^2+c^2}}\right|_0^{\infty}=\frac{1}{c}, \quad (44)$$

$$\int_0^{\infty}\frac{\rho d\rho}{\left(\rho^2+c^2\right)^{5/2}}=-\left.\frac{1}{3\left(\rho^2+c^2\right)^{3/2}}\right|_0^{\infty}=\frac{1}{3c^3}. \quad (45)$$

With the integral formulas of (44) and (45), the $Q_{iT}$ of (43) is integrated to yield $Q_{iT}=-4\pi\epsilon_0\kappa_3\nu$. Insertion of the explicit expression for $\nu$ from (33) yields

$$Q_{iT}=-\left(Q_b+Q_1+Q_2\right), \quad (46)$$

where

$$Q_b=8\pi a\left(b-a\right)\sigma_1\frac{\kappa_3}{\kappa_2},$$
$$Q_1=4\pi a^2\sigma_1,\quad Q_2=4\pi b^2\sigma_2.$$

The three quantities are identified as follow. The $Q_1$ and $Q_2$ are the "free charges" on the surfaces at $r=a$ and $r=b$, respectively. The $Q_b$ is the bound charge formed in the dielectric shell that surrounds the core.

### C. Particle dynamics

The true dynamics of a non-stationary particle involves electric field given by

$$\mathbf{E}_i=-\nabla V\left(\mathbf{R}_i,t\right)-\frac{\partial\mathbf{A}\left(\mathbf{R}_i,t\right)}{\partial t},$$

where both the scalar and vector potentials involve retarded time due to the finite speed at which the electromagnetic information travels. However, for the system considered here, where the distance between each conductor plates and the charged-particle are small, i.e., $h\lesssim 1\,\mathrm{mm}$, which is approximately three hundred billionth of a distance covered by the light in a second in vacuum, the dynamics of the particle can be approximated from

$$\mathbf{E}_i\approx-\nabla V\left(\mathbf{R}_i\right),$$

based on which assumption all of the electrostatic quantities had been derived previously. That said, the force

exerted on the charged-particle by the induced charges on the surfaces of the conductor plates is given by

$$\begin{aligned}\mathbf{F} &= \mathbf{F}_1 + \mathbf{F}_2 \\ &= -\frac{1}{2} Q_T \left( \int_{S_1} d\mathbf{E}_1 dS_1 + \int_{S_2} d\mathbf{E}_2 dS_2 \right), \end{aligned} \tag{47}$$

where $\mathbf{F}_1$ and $\mathbf{F}_2$ are the forces exerted on the particle respectively by the induced charges on the surface $S_1$ of the upper and $S_2$ of the lower conductor plates. The $(d\mathbf{E}_1, dS_1)$ and $(d\mathbf{E}_2, dS_2)$ are the respective differential electric fields and surface elements for the corresponding conductor plates. The effective charge, $Q_T$, carried by the particle is identical in magnitude to the $Q_{iT}$ of (46), but with opposite charge polarity. Thus, $Q_T = -Q_{iT}$ or

$$Q_T = 8\pi a \left(b - a\right) \sigma_1 \frac{\kappa_3}{\kappa_2} + 4\pi \left(a^2 \sigma_1 + b^2 \sigma_2\right). \tag{48}$$

The extra factor of $1/2$ in (47) comes from the fact that each parallel conductor plates sees only a hemisphere of the charged-particle; and, the negative sign is necessary for specifying correctly the direction of the forces exerted on the particle by the induced surface charges. For instance, if $Q_T$ and the induced surface charge density on $S_1$ have the same charge polarity, then the force between the two would be repulsive. Since the mass of the conductor plate is enormously larger than the mass of the charged-particle, it is the particle that effectively gets repulsed; and, hence, the negative sign in front of the factor of $1/2$. By the same token, if $Q_T$ and the induced surface charge density on $S_2$ have the same charge polarity, then the charged-particle would be repulsed away from the surface $S_2$; and, thus the negative sign in front of the factor of $1/2$. That said, in explicit forms, $\mathbf{F}_1$ and $\mathbf{F}_2$ are given by

$$\mathbf{F}_i = -\frac{Q_T}{8\pi\epsilon_3} \int_{\phi_i=0}^{2\pi} \int_{\rho_i=0}^{\rho} \frac{\varsigma_i \mathbf{R}_i \rho_i d\rho_i d\phi_i}{\left(\mathbf{R}_i \cdot \mathbf{R}_i\right)^{3/2}}, \tag{49}$$

where $i = (1, 2)$, $\varsigma_1 \equiv \sigma_{iup}$ of (41), $\varsigma_2 \equiv \sigma_{ilp}$ of (42), $\epsilon_3$ is the electric permittivity of the region $M_3$, and the explicit expression for $\mathbf{R}_i$, which defines the position of the $\varsigma_i$ associated with $dS_i$ as illustrated in Fig. 1(a), for $i = (1, 2)$ are given by

$$\mathbf{R}_1 = \mathbf{e}_x \rho_1 \cos\phi_1 + \mathbf{e}_y \rho_1 \sin\phi_1 + \mathbf{e}_z s \tag{50}$$

$$\mathbf{R}_2 = \mathbf{e}_x \rho_2 \cos\phi_2 + \mathbf{e}_y \rho_2 \sin\phi_2 - \mathbf{e}_z \left(h - s\right). \tag{51}$$

The force exerted on the particle by the induced charge on the surface of the upper conductor plate is obtained by inserting $\mathbf{R}_1$ of (50) into (49). This yields

$$\begin{aligned}\mathbf{F}_1 = -\frac{Q_T}{8\pi\epsilon_3} \int_{\phi_1=0}^{2\pi} \int_{\rho_1=0}^{\rho} \Bigg[ & \mathbf{e}_x \frac{\varsigma_1 \rho_1 \cos\phi_1}{\left(\rho_1^2 + s^2\right)^{3/2}} \\ & + \mathbf{e}_y \frac{\varsigma_1 \rho_1 \sin\phi_1}{\left(\rho_1^2 + s^2\right)^{3/2}} + \mathbf{e}_z \frac{\varsigma_1 s}{\left(\rho_1^2 + s^2\right)^{3/2}} \Bigg] \rho_1 d\rho_1 d\phi_1. \end{aligned} \tag{52}$$

The two terms in the integrand with $\cos\phi_1$ and $\sin\phi_1$ vanish when integrated over $d\phi$. Thus, (52) reduces to

$$\mathbf{F}_1 = -\mathbf{e}_z \frac{Q_T s}{4\epsilon_3} \int_0^{\rho} \frac{\sigma_{iup} \rho_1 d\rho_1}{\left(\rho_1^2 + s^2\right)^{3/2}}, \tag{53}$$

where $\varsigma_1 \equiv \sigma_{iup}$. Insertion of the explicit expression for $\sigma_{iup}$ from (41) into (53) yields

$$\begin{aligned}\mathbf{F}_1 = \mathbf{e}_z \frac{Q_T E_p s}{4} \int_0^{\rho} \Bigg[ & \frac{3b^3 s^2}{2\left(\rho_1^2 + s^2\right)^4} \\ & + \frac{2\nu s - b^3 E_p}{2E_p \left(\rho_1^2 + s^2\right)^3} - \frac{1}{\left(\rho_1^2 + s^2\right)^{3/2}} \Bigg] \rho_1 d\rho_1. \end{aligned} \tag{54}$$

Equation (54) involves the following type of integrals:

$$\int_0^{\rho} \frac{\rho_1 d\rho_1}{\left(\rho_1^2 + s^2\right)^4} = \frac{1}{6s^6} - \frac{1}{6\left(\rho^2 + s^2\right)^3}, \tag{55}$$

$$\int_0^{\rho} \frac{\rho_1 d\rho_1}{\left(\rho_1^2 + s^2\right)^3} = \frac{1}{4s^4} - \frac{1}{4\left(\rho^2 + s^2\right)^2}, \tag{56}$$

$$\int_0^{\rho} \frac{\rho_1 d\rho_1}{\left(\rho_1^2 + s^2\right)^{3/2}} = \frac{1}{s} - \frac{1}{\sqrt{\rho^2 + s^2}}. \tag{57}$$

Insertion of (55), (56), and (57) into (54) yields

$$\begin{aligned}\mathbf{F}_1 = \mathbf{e}_z \frac{Q_T E_p}{16} \Bigg[ & \frac{\nu}{E_p s^2} - \frac{\nu s^2}{E_p \left(\rho^2 + s^2\right)^2} + \frac{b^3}{2s^3} \\ & + \frac{b^3 s}{2\left(\rho^2 + s^2\right)^2} - \frac{b^3 s^3}{\left(\rho^2 + s^2\right)^3} + \frac{4s}{\sqrt{\rho^2 + s^2}} - 4 \Bigg], \end{aligned} \tag{58}$$

which is the force exerted on the charged-particle by the induced charges on the surface of the upper conductor plate.

The expression for the force exerted on the particle by the induced charges on the surface of the lower conductor plate is obtained by inserting $\mathbf{R}_2$ of (51) into (49). Repeating the similar procedure outlined in (52) and (53), one obtains

$$\mathbf{F}_2 = \mathbf{e}_z \frac{Q_T \left(h - s\right)}{4\epsilon_3} \int_0^{\rho} \frac{\sigma_{ilp} \rho_2 d\rho_2}{\left[\rho_2^2 + \left(h - s\right)^2\right]^{3/2}}. \tag{59}$$

Insertion of the explicit expression for $\sigma_{ilp}$ from (42) into (59) yields

$$\begin{aligned}\mathbf{F}_2 = \mathbf{e}_z \frac{Q_T E_p \left(h - s\right)}{4} \int_0^{\rho} \Bigg\{ & \frac{3b^3 \left(h - s\right)^2}{2\left[\rho_2^2 + \left(h - s\right)^2\right]^4} \\ & - \frac{2\nu\left(h - s\right) + b^3 E_p}{2E_p \left[\rho_2^2 + \left(h - s\right)^2\right]^3} - \frac{1}{\left[\rho_2^2 + \left(h - s\right)^2\right]^{3/2}} \Bigg\} \rho_2 d\rho_2. \end{aligned} \tag{60}$$

Using the integral formulas from (55), (56), and (57) with $s$ replaced by $h-s$, (60) becomes

$$\mathbf{F}_2 = \mathbf{e}_z \frac{Q_T E_p}{16} \left\{ \frac{\nu\,(h-s)^2}{E_p\left[\rho^2+(h-s)^2\right]^2} - \frac{\nu}{E_p\,(h-s)^2} + \frac{b^3}{2\,(h-s)^3} + \frac{b^3\,(h-s)}{2\left[\rho^2+(h-s)^2\right]^2} - \frac{b^3\,(h-s)^3}{\left[\rho^2+(h-s)^2\right]^3} + \frac{4\,(h-s)}{\sqrt{\rho^2+(h-s)^2}} - 4 \right\}, \tag{61}$$

which is the force exerted on the charged-particle by the induced charges on the surface of the lower conductor plate. For the parallel plate system, which is microscopically large, but macroscopically small, the forces in (58) and (61) can be approximated by making $\rho$ go to infinity. This approximation is certainly valid for very small charged-particles confined between large parallel conductor plates. In the limit $\rho$ goes to infinity, (58) and (61) simplify in form as

$$\mathbf{F}_1 = \mathbf{e}_z \frac{Q_T}{4}\left(\frac{\nu}{4s^2} + \frac{b^3 E_p}{8s^3} - E_p\right), \tag{62}$$

$$\mathbf{F}_2 = \mathbf{e}_z \frac{Q_T}{4}\left[\frac{b^3 E_p}{8\,(h-s)^3} - \frac{\nu}{4\,(h-s)^2} - E_p\right]. \tag{63}$$

Insertion of (62) and (63) into (47) yields the total force exerted on the charged-particle by the induced charges on the surfaces of parallel plate conductors. The result is

$$\mathbf{F} = \mathbf{e}_z \frac{Q_T}{32}\left[\frac{2\nu}{s^2} - \frac{2\nu}{(h-s)^2} + \frac{b^3 E_p}{s^3} + \frac{b^3 E_p}{(h-s)^3} - 16E_p\right].$$

If the gravitational effect is included, the force experienced by the particle is $\mathbf{F}_T = \mathbf{F} - \mathbf{e}_z mg$ or

$$\mathbf{F}_T = \mathbf{e}_z \left\{ \frac{Q_T}{32}\left[\frac{2\nu}{s^2} - \frac{2\nu}{(h-s)^2} + \frac{b^3 E_p}{s^3} + \frac{b^3 E_p}{(h-s)^3} - 16E_p\right] - mg \right\}, \tag{64}$$

where $m$ is the mass of the particle, $g = 9.8\,\mathrm{m\cdot s^{-2}}$ is the gravitational constant, and the gravitational force has been assumed to be in the $-\mathbf{e}_z$ direction.

The dynamics of oscillating charged-particle is given by

$$\mathbf{e}_z \frac{d}{dt}\left(\frac{mv}{\sqrt{1-\frac{v^2}{c^2}}}\right) = \mathbf{F}_T, \tag{65}$$

where $c = 3\times 10^8\,\mathrm{m\cdot s^{-1}}$ is the speed of light in vacuum. The left hand side of (65) can be differentiated to give

$$\mathbf{e}_z v \frac{d}{dt}\left(\frac{1}{\sqrt{1-\frac{v^2}{c^2}}}\right) + \frac{\dot{v}\mathbf{e}_z}{\sqrt{1-\frac{v^2}{c^2}}} = \frac{\mathbf{F}_T}{m}, \tag{66}$$

where $\dot{v} \equiv dv/dt$. Knowing that

$$\frac{d}{dt}\left(\frac{1}{\sqrt{1-\frac{v^2}{c^2}}}\right) = \frac{v\dot{v}}{c^2\left(1-\frac{v^2}{c^2}\right)^{3/2}},$$

equation (66) becomes

$$\frac{v^2\dot{v}\mathbf{e}_z}{c^2\left(1-\frac{v^2}{c^2}\right)^{3/2}} + \frac{\dot{v}\mathbf{e}_z}{\sqrt{1-\frac{v^2}{c^2}}} = \frac{\mathbf{F}_T}{m}.$$

Multiplying both sides by $c^2\left(1-v^2/c^2\right)^{3/2}$ yields

$$\dot{v}\mathbf{e}_z = \frac{\mathbf{F}_T}{m}\left(1-\frac{v^2}{c^2}\right)^{3/2}. \tag{67}$$

Since $v = \dot{s}$ and $\dot{v} = \ddot{s}$, (67) becomes

$$\ddot{s}\mathbf{e}_z = \frac{\mathbf{F}_T}{m}\left(1-\frac{\dot{s}^2}{c^2}\right)^{3/2},$$

where $\ddot{s} \equiv d^2s/dt^2$. With $\mathbf{F}_T$ explicitly inserted from (64), the expression for $\ddot{s}$ becomes

$$\ddot{s} = \left\{ \frac{Q_T}{32m}\left[\frac{2\nu}{s^2} - \frac{2\nu}{(h-s)^2} + \frac{b^3 E_p}{s^3} + \frac{b^3 E_p}{(h-s)^3} - 16E_p\right] - g \right\}\left(1-\frac{\dot{s}^2}{c^2}\right)^{3/2}, \tag{68}$$

where $\mathbf{e}_z$ has been dropped for convenience. It is convenient to re-express (68) in terms of the variable $z_d$ illustrated in Fig. 1(a). Two variables, $s$ and $z_d$, are related to each other by

$$s = z_d + b, \quad \dot{s} = \dot{z}_d, \quad \ddot{s} = \ddot{z}_d, \tag{69}$$

where $b$ is a constant. Hence, in terms of $z_d$, (68) becomes

$$\ddot{z}_d = \left(1-\frac{\dot{z}_d^2}{c^2}\right)^{3/2}\left\{ \frac{Q_T}{32m}\left[\frac{2\nu}{(z_d+b)^2} - \frac{2\nu}{(h-z_d-b)^2} + \frac{b^3 E_p}{(z_d+b)^3} + \frac{b^3 E_p}{(h-z_d-b)^3} - 16E_p\right] - g \right\}, \tag{70}$$

which result governs the dynamics of the oscillating charged-particle, subjected to high DC fields, at all speeds.

To solve and plot (70), the core-shell structured particle in Fig. 1 has been chosen to be the aluminum

nanoparticle, where the core is aluminum and the shell is aluminum oxide. The following parameter values have been assigned:

$$\begin{cases} \kappa_2 = 6, \quad \kappa_3 = 1, \\ a = 1.5\,\mu\text{m}, \quad h = 1\,\text{mm}, \\ b - a = 4\,\text{nm}, \\ V_T = 4.67\,\text{kV}, \quad V_L = 0\,\text{V}, \\ \sigma_1 = 141.47\,\mu\text{C}\cdot\text{m}^{-2}, \\ \sigma_2 = 1.53\,\text{pC}\cdot\text{m}^{-2}, \\ \rho_{m,1} = 2.7\,\text{kg}\cdot\text{m}^{-3}, \\ \rho_{m,2} = 3.8\,\text{kg}\cdot\text{m}^{-3}, \end{cases} \tag{71}$$

where $\rho_{m,1}$ and $\rho_{m,2}$ are mass densities of the aluminum core and the aluminum oxide, respectively. The thickness of aluminum oxide layer has been set at 4 nm, which is typical of aluminum nanoparticles[10]. Because aluminum oxide is a high-k dielectric material, i.e., $k_2 \sim 6$, the $\sigma_2$ has been chosen such that it is negligible compared to $\sigma_1$[11]. The values for the particle core diameter, the core surface charge density, and the DC bias voltage across the electrodes have been borrowed from Szirmai's experiment[3]. According to Szirmai, the spherical aluminum particle of $3\,\mu$m in diameter subjected to a DC field of $4.67\,\text{kV}\cdot\text{mm}^{-1}$ carries an estimated surface charge density of $4\times10^{-15}\,\text{C}$. For $a \approx 1.5\,\mu$m, $h = 1\,$mm, and $V_T - V_L = 4.67\,$kV, this corresponds to $\sigma_1 = 141.47\,\mu\text{C}\cdot\text{m}^{-2}$. The mass of the core-shell structured particle has been computed as

$$m = \underbrace{\frac{4}{3}\pi a^3 \rho_{m,1}}_{m_c} + \underbrace{\frac{4}{3}\pi\left(b^3 - a^3\right)\rho_{m,2}}_{m_s}, \tag{72}$$

where $m_c$ and $m_s$ represent the masses of the core and the shell, respectively. With values assigned for each of the parameters, (70) is solved via Runge-Kutta method subjected to the following initial conditions,

$$z_d(0) = h - 2b \quad \text{and} \quad \dot{z}_d(0) = 0, \tag{73}$$

which conditions are schematically illustrated in Fig. 2.

The particle position as a function of time corresponding to the parameter values defined in (71) is illustrated in Fig. 3(a). The core-shell structured charged-particle oscillates between the plane-parallel conductors that are biased with a DC voltage across the electrodes. It is noticed that the charged-particle rebounds at a point sufficiently away from the surface of the upper electrode, which is denoted by $z_d = 0$. The rebounding occurs approximately at $z_d \approx 0.0006\,$m. Considering the particle in Fig. 3(a) has a diameter of approximately $\sim 3\,\mu$m, this leaves a gap of approximately $\sim 600\,\mu$m between the surface of the upper electrode and the particle's uppermost surface. Such charged-particle oscillation, in which the rebounding occurs without touching the surface of the electrode, cannot be explained by the traditionally accepted idea where the charged-particle oscillation is attributed to the sign reversal occurring in the particle's charge polarity during the rebound between the two

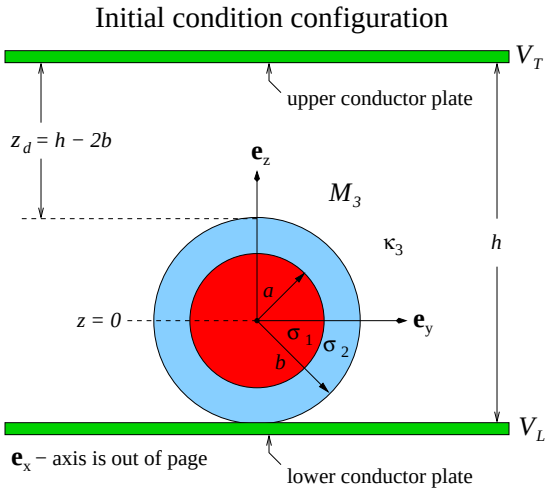


Figure 2: Schematic of initial conditions specified in (73).

electrodes, touching the surfaces of each electrodes as it rebounds. Since the oscillating charged-particle in Fig. 3(a) does not actually touch the surface of the rebounding upper electrode, the idea of sign reversal occurring in the particle's charge polarity between rebounds does not hold up; and, such idea or explanation cannot explain the physics of charged-particle oscillation subjected to a uniform DC fields.

The frequency of charged-particle oscillation depends on the strength of the DC field between the plane-parallel electrodes as well as on the charge carried by the particle. The electric field strength, $E_p$, can be increased either by decreasing the gap between the electrodes or by increasing the applied DC bias voltage across the electrodes. The increased electric field strength, in turn, increases the free charge density on the particle. According to Felici, the increase in the particle's free charge density, $\sigma_1$ and $\sigma_2$, is directly proportional to the strength of the electric field, implying $\sigma_1 \propto E_p$ and $\sigma_2 \propto E_p$[12]. Reducing the gap between the electrodes from 1 mm to $10\,\mu$m increases the strength of electric field by a factor of one hundred. According to Zouche and Lefort, the gap between a plane-parallel electrodes as small as $1\,\mu$m in vacuum, subjected to a vacuum pressure of $\sim 1.4\times10^{-4}\,$Pa (or $\sim 1\times10^{-6}\,$Torr), can support a DC bias voltage of approximately $\sim 3.85\,$kV before electrical breakdown takes place[13]. Therefore, it certainly is not unreasonable to apply a DC bias voltage of 4.67 kV across the electrode gap of $10\,\mu$m. The net charge on the particle gets increased by the same factor as that of electric field. Thus, for $h = 10\,\mu$m, the surface charge densities on the particle become $\sigma_1 = 0.014147\,\text{C}\cdot\text{m}^{-2}$ and $\sigma_2 = 153\,\text{pC}\cdot\text{m}^{-2}$.

The resulting charged-particle position as a function of time for $\sigma_1 = 0.014147\,\text{C}\cdot\text{m}^{-2}$ and $\sigma_2 = 153\,\text{pC}\cdot\text{m}^{-2}$ with $h = 10\,\mu$m is illustrated in Fig. 3(b). In Fig. 3(b), the rebounding occurs at approximately $z_d \approx -1.45\,\mu$m, which is below the $z_d = 0\,\mu$m. As mentioned previously,

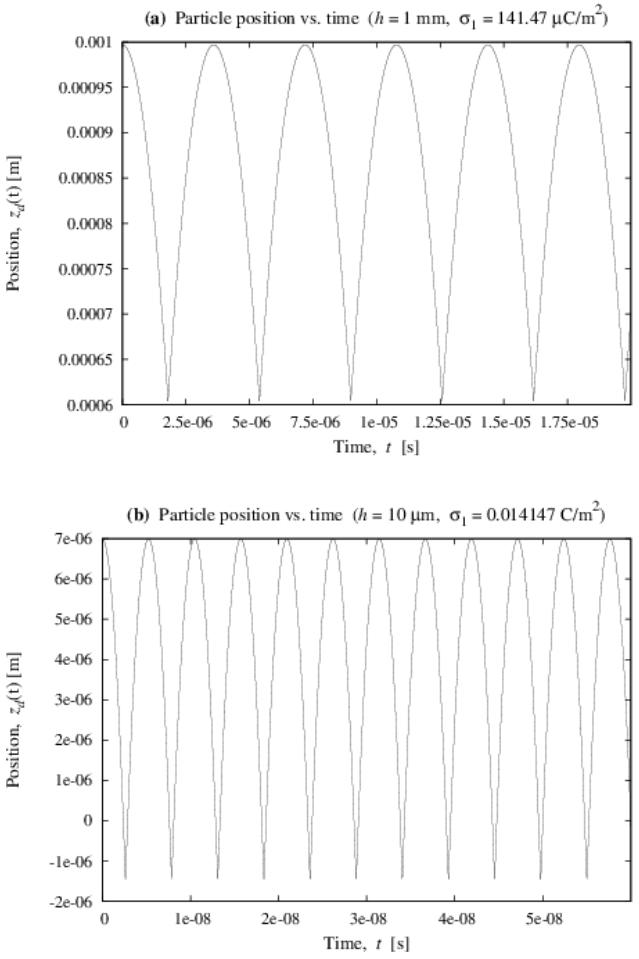


Figure 3: Particle position as a function of time. In (a), all of the parameter values are as defined in (71). In (b), $h = 10\,\mu$m, $\sigma_1 = 0.014147\,\mathrm{C}\cdot\mathrm{m}^{-2}$, and $\sigma_2 = 153\,\mathrm{pC}\cdot\mathrm{m}^{-2}$ and all other parameter values are identical to those defined in (71). The apparent rebounding at the negative $z_d$ in (b) disappears when the graph is re-plotted in terms of the particle's center of mass coordinate representation, $s$. Since $s = z_d + b$ from (69), in the $s$ representation, the plots in (a) and (b) are shifted by $b$.

$z_d = 0\,\mu$m is the surface of the upper electrode; and, the rebounding at $z_d \approx -1.45\,\mu$m gives an impression that charged-particle "digs" into the electrode before rebounding, which is not true. The fact that rebounding is portrayed to occur at the negative $z_d$ in the $z_d$ representation, hence giving a false impression of charged-particle momentarily digging into the surface of the electrode, can be attributed to the "point particle" picture which is inherent in the dynamical equation of (70). The equation of motion, (70), derived based on the Newtonian dynamics with relativistic corrections treats the core-shell structured charged-particle as a point particle, in which the mass and the charge density of the particle are assumed to be concentrated at the particle's center of mass. In this regards, when Fig. 3(b) is re-plotted in terms of the center of the mass coordinate, $s$, instead of the coordinate $z_d$, the rebounding is shown to occur at the surface of the upper electrode; and, the false impression of charged-particle digging into the surface of the electrode disappears altogether. This shift comes about because $s = z_d + b$ from (69); and, in the $s$ representation, the plots in Figs. 3(a) and (b) are shifted by $b$. That clarified, I shall continue to plot the position versus the time graph for the charged-particle in the $z_d$ representation throughout the work.

### D. Experiment apparatus

The experimental setup is illustrated in Fig. 4(a). The prototype for the particle confining chamber has been prepared using two petri dishes, as illustrated in Fig. 4(b). The upper and the lower electrodes have been produced by taping the bottoms of each plastic petri dishes with a copper tape. The aluminum balls of diameters ranging from approximately 1 mm to 4 mm were produced by folding the aluminum foil into the shape of a ball. The gap between the upper and the lower electrodes was measured to be approximately 3 cm. Due to relatively large separation distance between the two plane-parallel conductor electrodes, the Van de Graaff generator was used to sufficiently charge the aluminum balls and to create a DC electric field sufficiently large enough to satisfy the oscillation conditions,

$$\frac{2\nu}{15b^2} - \frac{32mg}{15Q_T} < E_p \quad \text{and} \quad \frac{2\nu}{15b^2} + \frac{32mg}{15Q_T} > -E_p,$$

which conditions are derived in the next section. The Van de Graaff generator used, although it is powerful enough to generate approximately $\sim 30$ kV of a DC voltage, it only generates current in the order of some microamperes. Therefore, the Van de Graaff generator is an "extremely low power consuming" power source which is capable of generating very high voltages. Although the figure shows only multiple aluminum balls present inside the chamber, the single aluminum ball case has also been tested using the identical setup.

### E. Principle behind the charged-particle oscillation

The observed charged-particle oscillation paths are schematically illustrated in Fig. 5. For the charged-particle oscillation of path 1, the rebound occurs at the surface of each electrodes. However, for the charged-particle oscillation involving the path 2, the rebound occurs at points sufficiently away from the surface of each electrodes. This latter oscillation mode cannot be explained by the traditional description in which the charged-particle oscillation is attributed to the sign reversal in the particle's charge polarity as it rebounds between the two electrodes. Because the particle does not actually touch the surfaces of the rebounding electrodes,

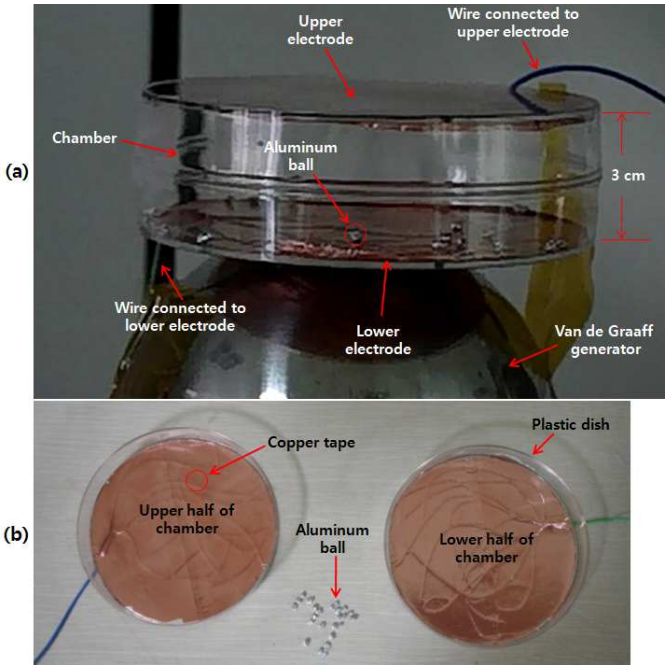


Figure 4: The experiment setup. (a) The prototype of charged-particle oscillator with one plane-parallel electrode connected to the positive end and the other one connected to the negative end of the Van de Graaff generator. (b) The particle confining chambers have been produced using two plastic petri dishes.

the idea of sign reversal occurring in the particle's charge polarity does not quite hold up for the charged-particle oscillation involving the path 2. The physics of charged-particle oscillation is inherent in the force expression of (64); and, it appears that the reversal in the sign of the particle's charge polarity, $Q_T$, is not responsible for the oscillatory behavior of the charged-particle in a uniform DC field. To see this, the force expression of (64),

$$\mathbf{F}_T = \mathbf{e}_z \left\{ \frac{Q_T}{32} \left[ \frac{2\nu}{s^2} - \frac{2\nu}{(h-s)^2} + \frac{b^3 E_p}{s^3} + \frac{b^3 E_p}{(h-s)^3} - 16E_p \right] - mg \right\},$$

is analyzed for situations where the particle is in close proximity to the surface of each electrodes.

When the charged-particle is in close proximity to the surface of upper electrode, $s$ becomes negligible compared to $h-s$ and the force experienced by the particle becomes

$$\mathbf{F}_T = \mathbf{e}_z \left[ \frac{Q_T}{32} \left( \frac{2\nu}{s^2} + \frac{b^3 E_p}{s^3} - 16E_p \right) - mg \right],$$

where $s \ll h$. When the particle is actually touching the surface of upper electrode, $s = b$; and, thus

$$\mathbf{F}_T = \mathbf{e}_z \underbrace{\left[ \frac{Q_T}{32} \left( \frac{2\nu}{b^2} - 15E_p \right) - mg \right]}_{F}. \tag{74}$$

For a positively charged particle, the oscillatory solution requires that $F < 0$ and this implies the condition,

$$\frac{Q_T}{32} \left( \frac{2\nu}{b^2} - 15E_p \right) - mg < 0$$

or

$$\frac{2\nu}{15b^2} - \frac{32mg}{15Q_T} < E_p. \tag{75}$$

Equation (75) is the condition for charged-particle oscillation and it can always be satisfied for a sufficiently large $E_p$. The requirement of $F < 0$ for the oscillatory solution comes from the fact that (74) is a second order ordinary differential equation,

$$m\frac{d^2 s}{dt^2} = \mathbf{e}_z \left[ \frac{Q_T}{32} \left( \frac{2\nu}{b^2} - 15E_p \right) - mg \right],$$

where the non-relativistic form has been used for the sake of simplicity. The solution for such differential equation is oscillatory when $F$ is negative.

When the charged-particle is in close proximity to the surface of lower electrode, $h-s$ becomes negligible compared to $s$; and, the force experienced by the particle becomes

$$\mathbf{F}_T = \mathbf{e}_z \left\{ \frac{Q_T}{32} \left[ -\frac{2\nu}{(h-s)^2} + \frac{b^3 E_p}{(h-s)^3} - 16E_p \right] - mg \right\},$$

where $s \approx h$. When the particle is actually touching the surface of lower electrode, $s = h - b$; and, the expression for $\mathbf{F}_T$ simplifies as

$$\mathbf{F}_T = -\mathbf{e}_z \underbrace{\left[ \frac{Q_T}{32} \left( \frac{2\nu}{b^2} + 15E_p \right) + mg \right]}_{G}.$$

For a positively charged particle, the oscillatory solution requires that $G > 0$; and, this implies

$$\frac{Q_T}{32} \left( \frac{2\nu}{b^2} + 15E_p \right) + mg > 0$$

or

$$\frac{2\nu}{15b^2} + \frac{32mg}{15Q_T} > -E_p. \tag{76}$$

Equation (76) is another condition for charged-particle oscillation and it can also be satisfied for $E_p$ that is sufficiently large.

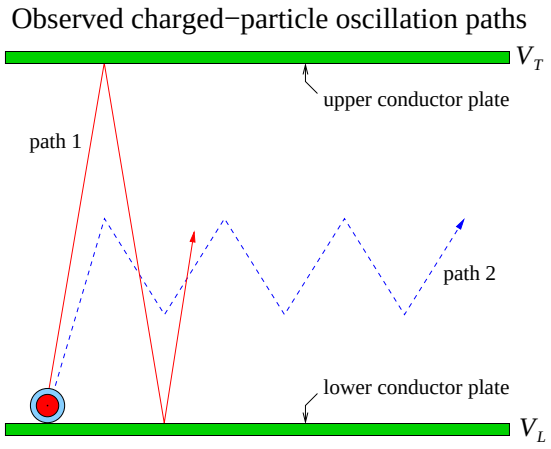


Figure 5: Observed paths of the charged-particle oscillation.

Comparing the two conditions, (75) and (76), one notices that if (75) is satisfied, then the latter condition, (76), is automatically satisfied. On the other hand, the sign of the charge, i.e., the sign of $Q_T$, remains fixed in both (75) and (76). Since the charged-particle oscillation in a uniform DC fields is solely due to the conditions of (75) and (76), in which equations the sign of $Q_T$ remains fixed, the traditionally accepted idea of sign reversal occurring in the particle's charge polarity during the rebounds does not hold up; and, such idea is unnecessary for the charged-particle oscillation in a uniform DC fields. Instead, the oscillatory behavior of a charged-particle in a uniform DC field requires sufficiently large electric field strength, $E_p$, to initiate the oscillation modes, as verified by experiments.

### F. Electromagnetic radiation

It is well known that the oscillating charged-particle radiates electromagnetic energy. With respect to the reference point on the surface of the upper conductor plate, the oscillating charged-particle has a dipole moment given by

$$\mathbf{p}_d = -\mathbf{e}_z Q_T s$$

where $\mathbf{p}_d \equiv \mathbf{p}_d(t)$, $s \equiv s(t)$ and the negative sign comes from the fact that the particle is perceived as residing in the negative $z$-axis to someone on the surface of the upper conductor plate. In terms of $z_d \equiv z_d(t)$ defined in (69), $\mathbf{p}_d$ becomes

$$\begin{aligned}\mathbf{p}_d &= -\mathbf{e}_z Q_T (z_d + b),\\ \ddot{\mathbf{p}}_d &= -\mathbf{e}_z Q_T \ddot{z}_d,\end{aligned}$$

where $b$ is a constant. The electromagnetic power radiated by an oscillating charged-particle, $P_{rad}$, is given by the Liénard formula,

$$\begin{aligned}P_{rad} &= \frac{1}{6\pi\epsilon_0 c^3}\left(1-\frac{\dot{z}_d^2}{c^2}\right)^{-3}\ddot{\mathbf{p}}_d\cdot\ddot{\mathbf{p}}_d\\ &= \frac{Q_T^2}{6\pi\epsilon_0 c^3}\left(1-\frac{\dot{z}_d^2}{c^2}\right)^{-3}\ddot{z}_d^2\end{aligned}$$

or

$$\begin{aligned}P_{rad} = \frac{Q_T^2}{6\pi\epsilon_0 c^3}\Bigg\{\frac{Q_T}{32m}\Bigg[&\frac{2\nu}{(z_d+b)^2}-\frac{2\nu}{(h-z_d-b)^2}\\ &+\frac{b^3E_p}{(z_d+b)^3}+\frac{b^3E_p}{(h-z_d-b)^3}-16E_p\Bigg]-g\Bigg\}^2,\end{aligned}\tag{77}$$

where (70) has been substituted in for $\ddot{z}_d$.

The Liénard radiation power corresponding to the charged-particle motion illustrated in Fig. 3(b) has been computed and the results are illustrated in Fig. 6. The first radiation pulse in Fig. 6(a) has been zoomed for a detailed view of the profile and this is illustrated in Fig. 6(b). The resulting electromagnetic radiation is emitted in train of pulses.

### G. X-ray laser

An X-ray laser (or Xaser) is a device that emits coherent electromagnetic radiation in the near X-ray or extreme ultraviolet region of the spectrum, which typically involves wavelength on the order of several or tens of nanometers. The oscillating single charged-particle in the DC voltage biased parallel-plate cavity is an ideal candidate for generating coherent electromagnetic radiation. Because such system involves an oscillating nanoparticle, in which the position and the velocity of the particle is simultaneously well defined and can be observed experimentally, the classical electrodynamics is sufficient to describe the physics. The following parameter values,

$$\begin{cases}\kappa_2 = 1, \quad \kappa_3 = 1,\\ a = 1\,\text{nm}, \quad h = 10\,\text{nm},\\ b-a = 0\,\text{nm},\\ V_T = 467\,\text{kV}, \quad V_L = 0\,\text{V},\\ \sigma_1 = 50\,\text{C}\cdot\text{m}^{-2},\\ \sigma_2 = 0\,\text{C}\cdot\text{m}^{-2},\\ \rho_{m,1} = 19.3\,\text{kg}\cdot\text{m}^{-3},\\ \rho_{m,2} = 0\,\text{kg}\cdot\text{m}^{-3},\end{cases}\tag{78}$$

have been chosen to obtain the results in Fig. 7. The mass density of $\rho_{m,1} = 19.3\,\text{kg}\cdot\text{m}^{-3}$ has been selected from that of the gold nanoparticle. The system emits train of electromagnetic pulses at the period of approximately $\sim 0.6\,\text{fs}$, which corresponds to the ultraviolet radiation of wavelength $\sim 190\,\text{nm}$. High radiation power in Figs. 7(c) and (d) is attributed to very high speed at which the charged-particle moves, Fig. 7(b). Because the particle cannot exceed the speed of light, it must release energy in the form of radiation; and, as the particle

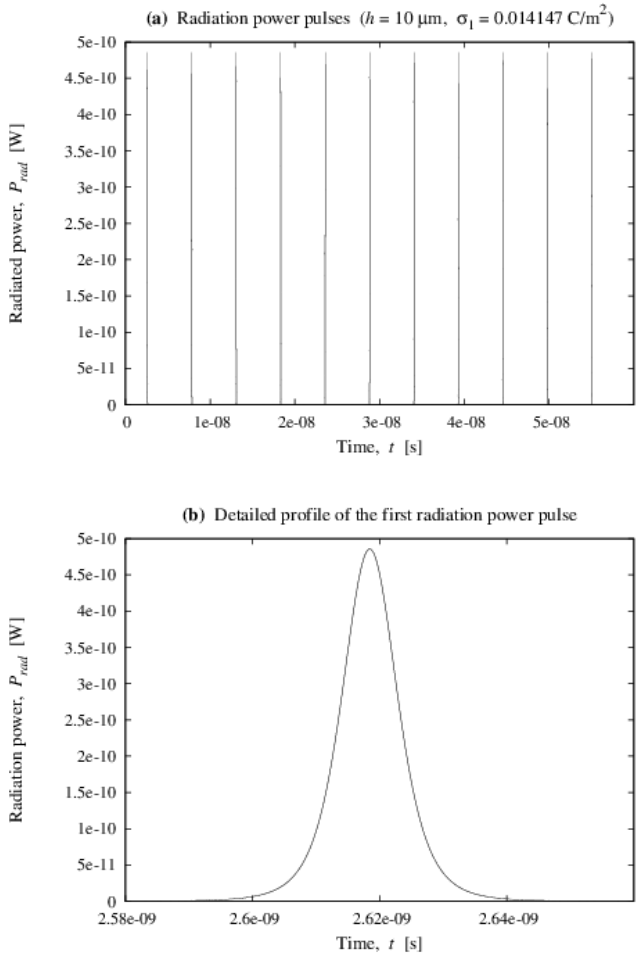


Figure 6: The Liénard radiation power corresponding to Fig. 3(b) is shown. (a) The radiation is emitted in train of pulses. (b) The first radiation pulse in (a) has been zoomed for a detailed view.

speed approaches the speed of light, the amount of energy released in the form of radiation can become enormous.

For the radiation at X-ray wavelengths, the parameters $a$, $V_T$, and $\sigma_1$ have been modified from (78) as $a = 0.5\,\text{nm}$, $V_T = 10\,\text{MV}$, and $\sigma_1 = 70\,\text{C}\cdot\text{m}^{-2}$. All other parameter values remain same as before. The results are illustrated in Fig. 8. The X-ray pulses are emitted at the period of approximately $\sim 0.1\,\text{fs}$, which corresponds to a wavelength of $\sim 30\,\text{nm}$. The significant increase in the radiation power, Figs. 8(c) and (d), is attributed to very high speed at which the charged-particle moves, Fig. 8(b).

The electromagnetic radiation behavior of an oscillating charged-particle system can be qualitatively compared with the radiation out of the fluorescent lamp filled with gases. The major differences between the two systems are in the size of the involved charged-particles as well as on the number of particles involved in the radiation. In the first system, the oscillating nanometer sized charged-particle is a classical particle; hence, its physics is described by the classical electrodynamics. The term, "classical particle," has been used to denote the nanometer sized oscillating charged-particle because its position and momentum can be specified simultaneously whereas a quantum particle cannot satisfy such conditions due to the uncertainty principle. Moreover, the nanometer sized oscillating charged-particle is a classical particle in the sense that it can be observed by "eyeball" experimentally. On the other hand, the atoms present in the fluorescent lamp in the form of gas are semi-classical particles and its physics involves quantum mechanical corrections.

The radiation out of the fluorescent lamp involves incoherent electromagnetic waves because each atoms in the gas acts as independent radiation sources. On the other hand, the oscillating nanometer sized "single" charged-particle system involves emission of coherent electromagnetic waves because the only source responsible for the radiation is the oscillating charged-particle itself. The excess free charges on the particle are in for a free ride, as the host goes through an oscillatory motion, where the host is the charged-particle, of course. One may envisage sailors on a boat, in which the boat moves up and down with the crest of the wave, with the system of excess free charges on an oscillating particle. The nanometer sized particle plays the role of the boat and the excess free charges on it take the role of the sailors. Just as each sailors on the waving boat can jump around, each charges on the particle can execute oscillations of their own. Such intrinsic oscillations by each charges on the particle result in fluctuations in the degree of coherence in the radiated waves. For many of the applications involving macroscopic coherent electromagnetic waves, however, such small fluctuations in the overall degree of coherence in the radiated waves are tolerable; and, the emitted electromagnetic waves are considered a coherent waves in the macroscopic sense.

Ostensibly, the light emitting device based on charged-particle oscillator is fundamentally different from the semiconductor or carbon nanotube based ones. In the latter technologies, the researches are mainly focused on lowering the electric fields and the field-emission threshold levels whereas, in the charged-particle oscillator technology, exactly the opposite is required. To generate electromagnetic waves in the visible or higher energies of the spectrum, in addition to the requirement of larger charge densities on the particle, the technology based on charged-particle oscillator calls for the stronger DC electric fields between the gap of plane-parallel electrodes without electrical breakdown. According to Zouache and Lefort, the process initiating discharge in vacuum is the electronic emission, which depends strongly on the strength of electric field[13]. The requirement for maintaining high DC electric fields in the gap of plane-parallel electrodes without electrical breakdown, therefore, demands electrodes with high field-emission threshold levels. Such property in an electrode is intrinsically tied to the work function of the electrode material[14]. For instance, in the report by Zouache and Lefort, the electrical breakdown voltage for a silver elec-

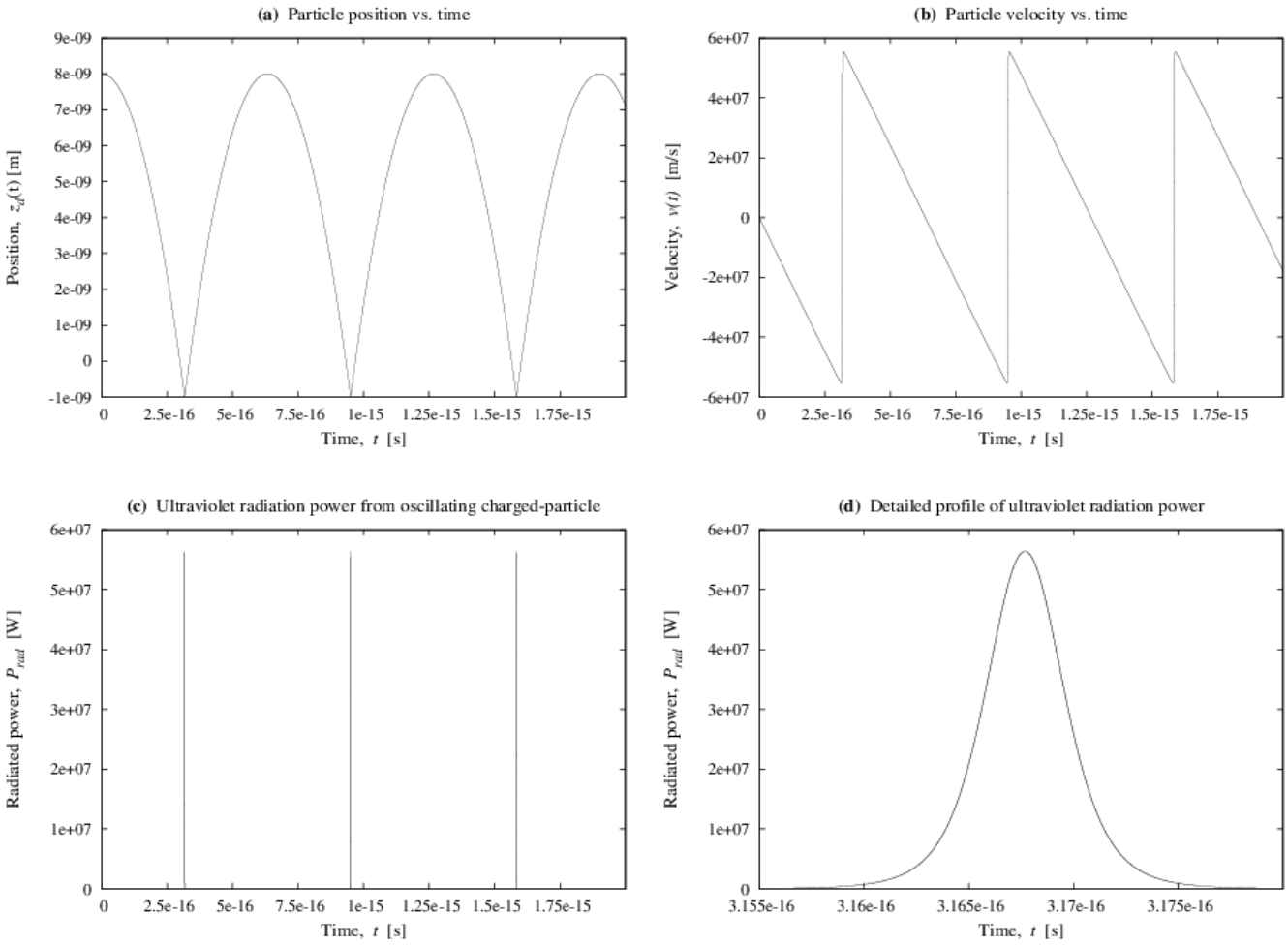


Figure 7: Dynamics of charged-particle with parameter values defined in (78). (a) Particle position as a function of time. (b) Particle velocity as a function on time. (c) Train of radiation pulses emitted by oscillating charged-particle. (d) The first radiation pulse in (c) has been zoomed for a detailed view.

trode has been increased from approximately $\sim 1.42\,\text{kV}$ to $\sim 3.85\,\text{kV}$ by mixing silver with nickel at the composition of Ag(60):Ni(40). Considering that the work function for the nickel ranges from 5.04 eV to 5.35 eV whereas the one for the silver ranges from 4.52 eV to 4.74 eV, depending on the orientation of the crystalline structure, the increased electrical breakdown voltage in the report by Zouache and Lefort can be attributed to the increased work function in the electrodes[14,15].

Unlike the light emitting devices based on semiconductor technologies, which involves small voltages but significant amount of currents, the technology based on charged-particle oscillator, such as the one presented in this work, involves insignificant amount of currents which is typically in the order of some pico-amperes. As a result, the ohmic power loses are insignificant in the presented radiation device based on charged-particle oscillator; and, the plane-parallel electrodes are not necessarily required to be selected from the best conductors available. However, because such technology requires high DC electric fields, conductive electrodes with high field-emission threshold properties are required. The oscillating charged-particle, on the other hand, is required to be selected from materials with low field-emission threshold properties compared to that of the electrodes, which require high field-emission threshold levels.

In principle, if there are many positively (or negatively) charged-particles in the space between the plane-parallel electrodes, then such system represents the plasma configuration. Therefore, effects observed in the plasma system can be regarded as a manifestation of the effects predicted by single charged-particle system considered here. One such manifestation is associated with the charged-particle oscillation between the two electrodes. As the charged-particle oscillates between the two plane-parallel electrodes, the currents in the electrodes get varied; and, such variations in each electrodes' current must have a profile which closely resembles the charged-particle's position versus the time graph. This must be so because it is the oscillating charged-particle that perturbs the oth-

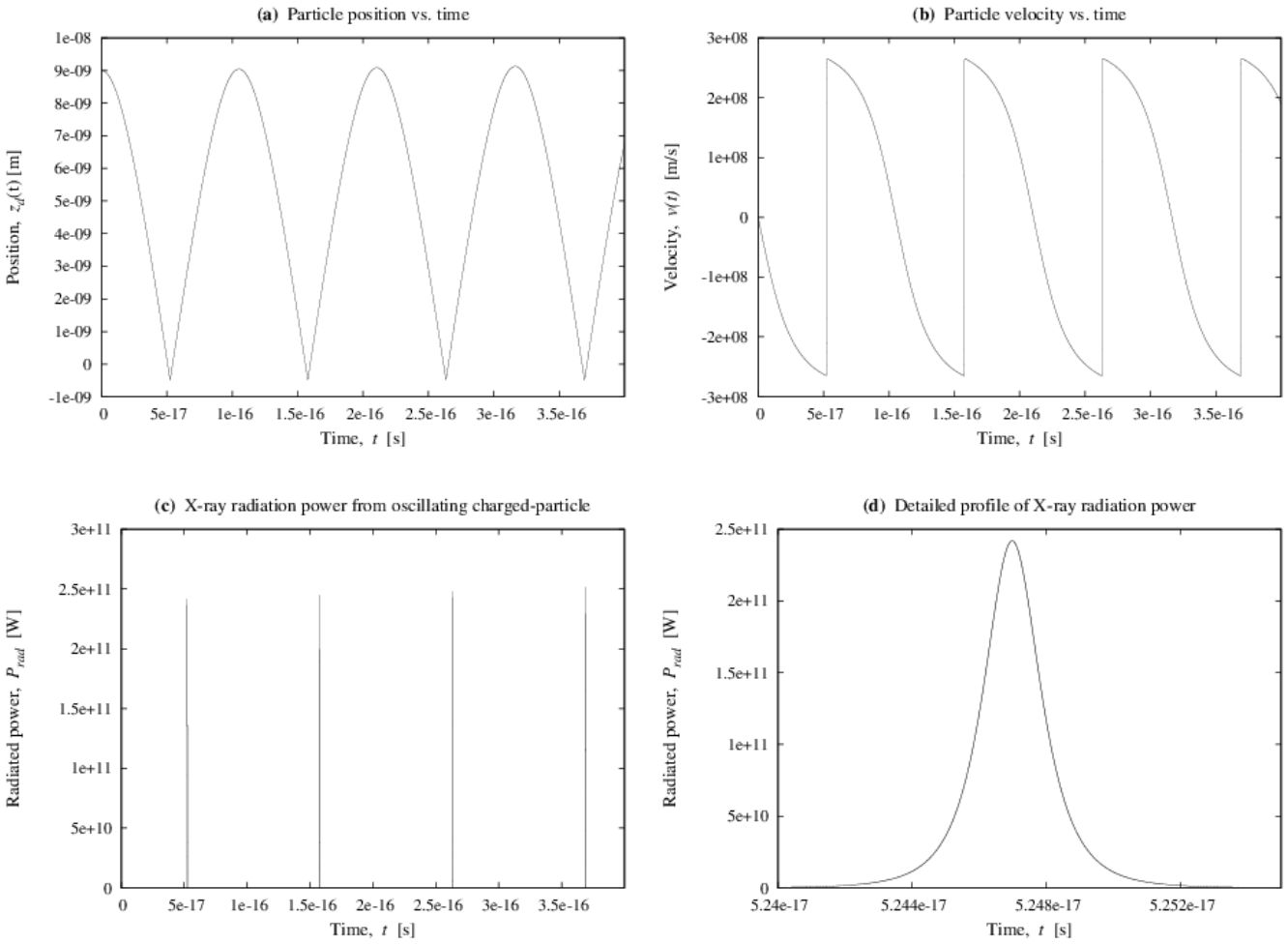


Figure 8: Dynamics of charged-particle is illustrated. For the plots, $a = 0.5\,\text{nm}$, $V_T = 10\,\text{MV}$, $\sigma_1 = 70\,\text{C}\cdot\text{m}^{-2}$ and all other parameter values are same as those defined in (78). (a) Particle position as a function of time. (b) Particle velocity as a function on time. (c) Train of radiation pulses emitted by oscillating charged-particle. (d) The first radiation pulse in (c) has been zoomed for a detailed view.

erwise constant current in each of the electrodes. For instance, if there is no charged-particle oscillation between the electrodes, then the current in each electrodes would be a constant with no variations what so ever; unless, of course, there are other dominant mechanisms that cause variations in the electrode's current. Gyergyek et al. measured the current variations in the electrode for a plasma system and obtained the current versus time profile which is remarkably similar to the charged-particle's position versus time plot illustrated Fig. 3[16]. The current versus time profile of their measurement shows a cusp at the bottom and a rounded top, which is exactly the kind of a shape predicted by (70) for the charged-particle's position versus time plot, as illustrated in Fig. 3. Another prediction from a single, charged-particle, oscillator system which gets manifested in the plasma comes from the location of where the glow or radiation is predicted to occur. For a single, positively charged, oscillating charged-particle considered here, pulses of radiation are emitted precisely at one of the electrodes. For a positively charged particle, this occurs near the electrode with higher potential; and, this is illustrated in Figs. 6, 7, and 8. For a negatively charged particle, although the plots for this particular case have not been provided, it shows that pulses of radiation are emitted near the electrode with lower potential. Such predictions are consistent with the experimentally observed "DC glow discharge" phenomenon[17]. Finally, the dynamics of charged-particle oscillation presented in this work describes the behavior of self-oscillating positively charged dust particles observed in a cross-sheath between the magnetized double plasmas with different potentials separated vertically by the horizontal magnetic field[18–20].

## III. CONCLUDING REMARKS

The oscillating behavior of a charged-particle inside the DC voltage biased plane-parallel conductors has been investigated. Contrary to the traditional belief wherein the charged-particle oscillation is attributed to the reversal in the sign of the particle's charge polarity as it rebounds between the two electrodes, the analytic description of the phenomenon presented here reveals that such condition is unnecessary for the charged-particle oscillation. The physics of charged-particle oscillation is inherent in the force expression of (64); and, the oscillatory behavior of a charged-particle in a uniform DC fields has nothing to do with the sign of the particle's charge polarity. The oscillatory condition for a charged-particle in a uniform DC field requires a sufficiently large electric fields, $E_p$, which must simultaneously satisfy the conditions specified in (75) and (76). It has been found that if the condition of (75) is satisfied by $E_p$, then the remaining condition, (76), is automatically satisfied by the same electric field; therefore, the charged-particle is guaranteed to oscillate in a uniform DC field for sufficiently large electric fields. Because the particle's charge polarity, i.e., the sign of $Q_T$, is identical and remains invariant in (75) and (76), it cannot be attributed to explain the oscillatory behavior of the charged-particle in a uniform DC fields, contrary to the traditional belief. Moreover, the traditional interpretation of the phenomenon fails to explain the observed oscillatory charged-particle motion which involves the path 2 illustrated in Fig. 5.

The oscillating charged-particle system emits train of electromagnetic radiation pulses; and, the frequency of emitted radiation is controlled by the DC bias voltage across the plane-parallel conductors. Since the system involves a spatially oscillating charged-particle, it represents a natural prototype for illuminating electric dipole radiation. Because the position and the velocity of an oscillating, nanometer sized, charged-particle are both well defined simultaneously and can be observed experimentally, the configuration is necessarily a classical system; and, the physics in such system is within the realm of classical electrodynamics. With parameter values appropriately chosen, (78) for instance, the "one particle" charged-particle oscillator system is predicted to generate the coherent electromagnetic waves in the microwave to the X-ray regions of the spectrum, which includes the technologically important terahertz, the infrared, the visible, and the ultraviolet wavelengths of the spectrum.

## IV. ACKNOWLEDGMENTS

The author acknowledges the support for this work provided by Samsung Electronics Co., Ltd. The author would also like to thank the community of LyX, Xfig, gnuplot, gfortran, and all other opensource developers, without whose generous contributions, the preparation of this manuscript would have been a mammoth task.

* Electronic address: sungnae.cho@samsung.com


[1] R. Tobazeon, J. Phys. D: Appl. Phys. **29**, 2595-2608 (1996).

[2] L. Musinski, T. Liu, B. Gilchrist, and A. Gallimore, J. Electrostatics **67**, 54-61 (2009).

[3] S. Szirmai, Industry Applications Conference, 2000. Conference Record of the 2000 IEEE (Rome, Italy) **2**, 851 (2000).

[4] Th. Trottenberg, H. Kersten, and H. Neumann, New J. Phys. **10**, 063012 (2008).

[5] L. Musinski, T. Liu, B. Gilchrist, A. Gallimore, M. Keidar, Experimental results and modeling advances in the study of nanoparticle field extraction thruster, in: AIAA-2007-5254, 43rd AIAA/ASME/SAE/ASEE Joint Propulsion Conference, Cincinnati, OH, July 8–11, (2007).

[6] L. Musinski, T. Liu, B. Gilchrist, A. Gallimore, M. Keidar, Nanoparticle field extraction thruster (nanoFET): design and results of the microparticle emitter prototype, in: International Electric Propulsion Conference, Florence, Italy, September 17–20, (2007).

[7] T. Liu, L. Musinski, P. Patel, A. Gallimore, B. Gilchrist, M. Keidar, Nanoparticle electric propulsion for space exploration, in: Space Technology and Applications International Forum, Albuquerque, NM, February 11–15, (2007).

[8] I. Eu, L. Musinski, T. Liu, A. Deng Di, D. Morris, J. Millunchick, B. Gilchrist, G. Gallimore, Inkless deposition of microparticles by electrostatic acceleration for materials processing, in: AVS 55th International Symposium and Exhibition, Boston MA, October 19–24, (2008).

[9] V. Tulagin, J. Opt. Soc. Am. **59** (3), 328-331 (1969).

[10] K. Tamura, Y. Kimura, H. Suzuki, O. Kido, T. Sato, T. Tanigaki, M. Kurumada, Y. Saito, and C. Kaito, Jpn. J. Appl. Phys. **42**, 7489-7492 (2003).

[11] R. Sohal, G. Lupina, O. Seifarth, P. Zaumseil, and C. Walczyk, Surface Science **604**, 276-282 (2010).

[12] N. Felici, Forces et Charges de Petits Objets en Contact Avec une Electrode Affectee d'um Champ Electriquie, Revue Generale d'Electricite 75 (1966), pp. 1145–1160.

[13] N. Zouache and A. Lefort, IEEE Trans. Dielectr. Electr. Insul., **4** (4), 358-364 (1997).

[14] H. Michaelson, J. Appl. Phys. **48**, 4729 (1977).

[15] D. Lide, CRC Handbook of Chemistry and Physics: A Ready-Reference Book of Chemical and Physical Data, 89th Edition (2008); ISBN: 9781420066791.

[16] T. Gyergyek, M. Cercek, M. Stanojevic, and N. Jelic, J. Phys. D: Appl. Phys. **27**, 2080-2094 (1994).

[17] B. Chiad, T. Al-zubaydi, M. Khalaf, and A. Khudiar, J. Optoelectron. Bio. Mater. **1** (3), 255-262 (2009).

[18] S. Nunomura, T. Misawa, N. Ohno, and S. Takamura, Phys. Rev. Lett. **83** (10), 1970-1973 (199).

[19] C. Ticos, P. Smith, and P. Shukla, Phys. Lett. A **319**, 504-509 (2003).

[20] S. Iizuka and T. Gohda, J. Plasma Fusion Res. **8**, 269-272 (2008).